Article

Multivariate Analysis of Individual Bacterial Outer Membrane Vesicles Using Fluorescence Microscopy

Aarshi N. Singh, Justin B Nice, Meishan Wu, Angela C. Brown, and Nathan J. Wittenberg*

Read Online

| ACCESS | | Metrics & More | | Article Recommendations | | Supporting Information |

ABSTRACT: Gram-negative bacteria produce outer membrane vesicles (OMVs) that play a critical role in cell−cell communication and virulence. OMVs have emerged as promising therapeutic agents for various biological applications such as vaccines and targeted drug delivery. However, the full potential of OMVs is currently constrained by inherent heterogeneities, such as size and cargo differences, and traditional ensemble assays are limited in their ability to reveal OMV heterogeneity. To overcome this issue, we devised an innovative approach enabling the identification of various characteristics of individual OMVs. This method, employing fluorescence microscopy, facilitates the detection of variations in size and surface markers. To demonstrate our method, we utilize the oral bacterium *Aggregatibacter actinomycetemcomitans* (*A. actinomycetemcomitans*) which produces OMVs with a bimodal size distribution. As part of its virulence, *A. actinomycetemcomitans* secretes leukotoxin (LtxA) in two forms: soluble and surface associated with the OMVs. We observed a correlation between the size and toxin presence where larger OMVs were much more likely to possess LtxA compared to the smaller OMVs. In addition, we noted that, among the smallest OMVs (<100 nm diameter), the fractions that are toxin positive range from 0 to 30%, while the largest OMVs (>200 nm diameter) are between 70 and 100% toxin positive.

KEYWORDS: *bacterial outer membrane vesicles, toxin sorting, single-vesicle analysis, OMV sizing, single-OMV heterogeneity*
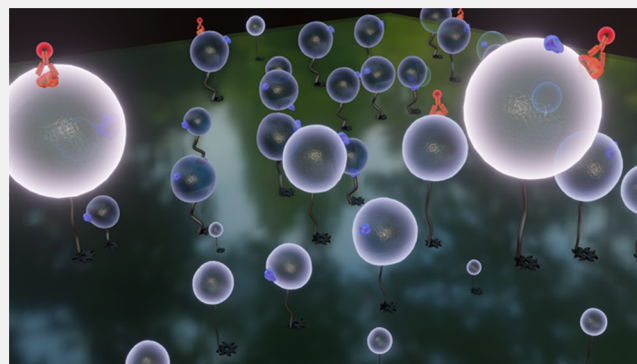
INTRODUCTION

Membrane-bound nanostructures are ubiquitous across all domains of life. Extracellular vesicles (EVs), such as outer membrane vesicles (OMVs) produced by Gram-negative bacteria, are a notable example of these structures. OMVs are spherical, bound by a lipid bilayer, and composed of various components, including lipids, membrane proteins, and other biomolecules derived from the outer membrane of the bacteria.[1−3] OMVs transport a range of diverse cargo such as nucleic acids, proteins, and toxins, which play crucial roles in various biological functions of OMVs. While non-pathogenic bacterial OMVs share functions with eukaryotic EVs, such as cellular communication and removal of unwanted components, pathogenic bacterial OMVs have a unique role in transporting toxins and other virulence factors to the host cell and facilitating the spread of disease.[4−8]

Although OMVs play a significant role in virulence and pathogenesis, certain features provide advantages for their use in various biotechnologies. Previously, an OMV-based vaccine has been approved for use for meningococcal disease,[9] and their small size, biological nature, and diverse surface antigens make them attractive targets for the development of other vaccines as well.[10,11] Furthermore, recent studies have shown

that OMVs can be bioengineered to deliver cytotoxic payloads directly to cancer cells, making them a promising tool for targeted cancer therapy.[12,13] Moreover, Kim et al. demonstrated that bioengineered OMVs can effectively reduce tumors even in the absence of a cytotoxic payload, indicating their potential as a standalone therapeutic agent, further highlighting the potential of OMVs.[14] In addition OMVs have also shown promise as carriers for antibiotics, enzymes, and use as diagnostic agents.[15−17] Nonetheless, owing to the inherent heterogeneity of OMVs, their complete utilization as therapeutics faces limitations, underscoring the need for further research and exploration.

OMVs exhibit heterogeneity encompassing variations in size, protein composition, and encapsulated cargo.[18,19] The intriguing heterogeneities observed in OMV structure and composition suggest that there may be significant differences in
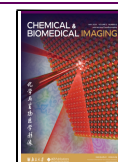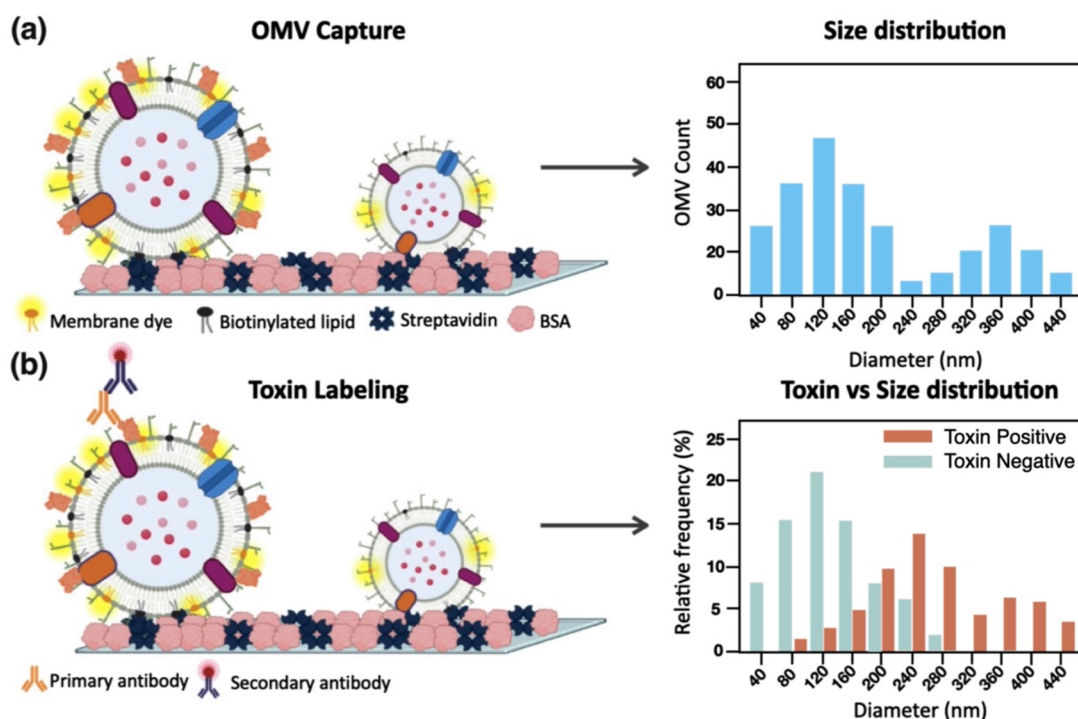
Figure 1. Schematic illustration of the assay: (a) OMVs are biotinylated and fluorescently labeled with a membrane dye and then immobilized on a glass surface, and their integrated fluorescence intensities are measured to generate their size distribution. (b) A toxin-specific antibody is introduced into the chamber and labeled with a fluorescent secondary antibody. The OMVs are categorized as toxin-positive and toxin-negative, and the size-based toxin distribution is determined. The histograms shown are for illustrative purposes.

function and immunological properties between different types of OMVs. While the entry of OMVs into cells through various mechanisms has been widely acknowledged,[20−23] it was not until a recent study by Turner et al. that the influence of the size of *Helicobacter pylori* OMVs on their entry into epithelial cells was revealed.[24] Specifically, smaller OMVs (20−100 nm) enter through caveolin-mediated endocytosis, whereas larger OMVs (90−450 nm) enter through macropinocytosis and endocytosis.[24] Additionally, protein heterogeneity was noted within the OMV population, with smaller OMVs containing proteins that were absent in the larger ones.[24] These findings underscore the significance of investigating and comprehending the heterogeneity present within a population of OMVs.

Despite the potential significance of OMV heterogeneity in determining their function and potential applications in vaccine development and other biomedical areas, the lack of research focused on characterizing the heterogeneities within an OMV population is a major limitation. This lack of research is primarily due to the limited analytical methods currently available for characterizing the heterogeneities within an OMV population. Ensemble assays such as ELISA and Western blots can provide information about the overall composition of OMV populations; however, they are unable to detect individual OMV heterogeneities.[19,25−28] In addition, to detect size-based heterogeneities, the OMV populations need to be separated using either the traditional density gradient ultra-centrifugation[24] or size exclusion chromatography (SEC) methods[29] which can be time-consuming and can add to the cost of the method. Recently, mass spectrometry has also been employed for OMV proteomics analysis.[30−33] However, it is important to note that this technique analyzes OMV ensembles and can be time- and cost-intensive, and it may necessitate specialized instrumentation. Methods such as

nanoparticle tracking analysis (NTA) and tunable resistance pulse sensing (TRPS) are also commonly used to analyze single-OMV size and concentration.[34−38] While both are sophisticated analytical techniques, they have limitations as well. NTA has its strengths in analyzing the size of OMVs and assessing their aggregation tendencies. However, when dealing with multiple overlapping sizes, its ability to distinguish and detect individual particles may be challenged. TRPS has its advantages, but it is constrained by the nanopore size range. Consequently, when dealing with highly polydisperse samples, determining the size of OMVs can become challenging.

To comprehend OMV heterogeneity, single-particle methods, such as flow cytometry[24,39,40] and electron micros-copy,[41−43] can also be used. However, these methods do come with certain limitations that can hinder their effectiveness. For example, flow cytometry operates on a continuous flow of OMVs, which makes it difficult to backtrack or perform additional analysis once heterogeneity is observed. Furthermore, flow cytometry requires special instrumental modifications to analyze nanoscale particles. Electron micros-copy, on the other hand, can exhibit sample preparation artifacts and may not accurately represent the native structure of OMVs. To overcome the challenges posed by specialized equipment, high costs, and technical expertise required by existing OMV analysis techniques, there is an urgent need to develop new methods that can utilize general laboratory equipment.

Optical microscopy is a powerful tool to analyze OMVs,[20,22,28,44,45] but it has a limitation where OMVs smaller than ∼200−400 nm appear as diffraction-limited spots and cannot be optically sized, due to which, any size-based heterogeneities can be masked. Previously, single-particle fluorescence sizing emerged as an alternative to determine

the size of nanoparticles smaller than 200 nm.[46] However, this method was previously employed with synthetic nanoparticles, like liposomes, which do not possess the intricate matrix associated with OMVs and potential aggregation. Here, we present an approach for multivariate analysis of single OMVs using fluorescence microscopy. Our method, illustrated in Figure 1, enables simultaneous detection of both the size and surface toxin/protein content on individual OMVs, providing a comprehensive characterization of these complex nanovesicles. Our analysis involves two steps. First, we captured biotinylated OMVs on a streptavidin-passivated glass surface and characterized their size based on integrated fluorescence intensity (Figure 1a). Second, we used a toxin-specific antibody to categorize the OMVs into two groups, toxin-positive and toxin-negative, and then determined the size distribution of each group (Figure 1b). Traditional techniques typically concentrate on examining either the protein or lipid aspects of OMVs in isolation. In contrast, our innovative approach centers on employing double staining methods that allow for the concurrent assessment of multiple variables such as size and the presence of toxins/proteins. This multivariate analysis enables a deeper and more holistic comprehension of OMV composition and structure, facilitating the extraction of valuable insights.

◼ METHODS

Reagent and Chemicals

1,2-Dipalmitoyl-*sn*-glycero-3-phosphoethanolamine-*N*-(cap biotinyl) (biotin cap-PE) was purchased from Avanti Polar Lipids. Streptavidin was purchased from New England Biolabs. Fatty-acid-free bovine serum albumin (BSA) and NeutrAvidin were purchased from Sigma-Aldrich. Anti-LtxA antibody was collected from the supernatant of hybridoma cell line LTA835, gifted by Dr. Edward T. Lally, University of Pennsylvania, grown in serum-free medium; the antibody was purified using a protein-G column. Anti-OmpA rabbit polyclonal antibody was purchased from Antibody Research Corporation. Secondary antibody with an Alexa-488 label was purchased from Abcam. Dimethyl sulfoxide (DMSO) was purchased from Sigma-Aldrich. DiI and DiO membrane labels were purchased from Invitrogen, ThermoFisher. All experiments were performed in Tris buffer composed of 150 mM NaCl and 10 mM Tris-base (pH 7.0).

Purification and Lipid Content Measurement of OMVs

A. actinomycetemcomitans strains JP2 and AA1704 were grown in trypticase soy broth (30 g/L, BD Biosciences, Franklin Lakes NJ) and yeast extract (6 g/L, BD Biosciences), supplemented with 0.4% sodium bicarbonate (Fisher Scientific, Hampton, NH, USA), 0.8% dextrose (BD Biosciences), 5 μg/mL vancomycin (Sigma-Aldrich, St. Louis, MO, USA), and 75 μg/mL bacitracin (Sigma-Aldrich). A starter culture of 100 mL was grown for 16 h in a candle jar, and then, 30 mL was inoculated into a 500 mL mixed media culture and allowed to grow for 24 h at 37 °C. The bacteria were centrifuged at 10,000 × g for 10 min and then again at the same speed for 5 min, followed by filtration through a 0.45 μm filter. This supernatant was then ultracentrifuged at 105,000 × g for 30 min, resuspended in PBS (pH 7.4), and ultracentrifuged again. The final pellet was resuspended in PBS. To confirm that the observed OMVs were indeed of bacterial origin, specifically *A. actinomycetemcomitans*, we conducted a negative control in which the culture media was not inoculated with *A. actinomycetemcomitans*, while still adhering to the complete OMV purification protocol and subjecting the final media to DLS. In addition, we conducted experiments using fetal bovine serum (FBS) media on DLA as an additional negative control. This additional control was employed to provide further evidence confirming that the observed OMVs did indeed originate from *A. actinomycetemcomitans* (Figure S1).

Escherichia coli JC8031 consisted of 10 mL of Luria−Bertani broth (Lennox, Invitrogen) with 100 μL of frozen stock, grown for 8 to 12 h at 37 °C and under constant shaking at 175 rpm. The starter culture is then transferred into a baffled flask with larger volume, diluted with media in 1:100 ratio, and grown under the same temperature or speed setting until the late exponential phase. The bacteria culture was centrifuged twice at 10,000 × g for 10 min and then filtered through a 0.45 μm filter to separate bacteria from supernatant. The supernatant was concentrated to approximately 150 mL before ultracentrifuging twice at 150,000 × g for 60 m. The pellet was resuspended using 1 mL of phosphate buffer saline (pH 7.4) and stored in a sterile Eppendorf tube. The liquid content was then centrifuged at 5000 × g for 5 min to remove impurities. Purified OMVs were at −20 °C until further use.

The lipid content was assessed by comparing the fluorescence intensity with a calibration curve generated using liposomes of known concentrations. Liposomes composed of 100% 1-palmitoyl-2-oleoyl-glycero-3-phosphocholine (POPC) were synthesized using the thin film method, hydrated in PBS, and extruded to 100 nm. The liposomes and OMVs were serially diluted, and 5 μL of the lipophilic dye, FM 4-64 (ThermoFisher), was added to each and incubated for 20 s. The fluorescence of all samples was quantified using a fluorometer with an excitation wavelength of 515 nm and an emission wavelength of 640 nm.

OMV Membrane Labeling and Biotinylation

To label the OMVs with fluorescent membrane dye, we utilized the lipophilic membrane dye DiI. Twenty μM of DiI dissolved in ethanol was added to the OMVs and incubated for 1 h at 37 °C to ensure optimal labeling efficiency. Additionally, we biotinylated the OMVs using biotincap-PE. To achieve this, we prepared biotin cap-PE in DMSO and then added 20 μM of the stock to the OMVs, which were then incubated at 37 °C for 1 h.

Scanning Electron Microscopy of OMVs

In addition, OMVs were characterized using scanning electron microscopy. OMVs were dried and fixed with Karnovsky's fixative on plasma-cleaned glass slides (Electron Microscopy Sciences, Hatfield, PA). Following this, the OMVs were dehydrated using a series of ethanol solutions (35%, 70%, 85%, 95%, and 100%), then a 50% hexamethyldisilazane (HDMS)/50% ethanol solution, and finally 100% HDMS. The samples were coated with iridium before being scanned with a Hitachi 4300 scanning electron microscope at a 3 kV accelerating voltage. Two distinct size populations of OMVs were observed by SEM, as shown in Figure S2.

Dynamic Light Scattering (DLS) of OMVs

OMV diameters were measured using dynamic light scattering (DLS). OMVs were diluted to 1:100 dilution factor in Tris buffer. DLS measurements were collected using the ALV/CGS-3 Compact Goniometer System spectrometer. The data was collected in triplicate for 120 s at the wavelength of 632.8 nm and a 90° scattering angle. ALV software number-weighted regularized fit with an allowed membrane thickness ($r*$) of 5 nm was used to determine the size distribution. A weighted average was calculated to obtain the mean radius for fluorescence microscopy particle sizing.

Antibody Passivation for OMV Surface Heterogeneity

Clean glass coverslips (2% SDS and UV/ozone treated) were passivated with either Anti-OmpA antibody or Anti-LtxA antibody (1:100 dilution) prepared in 1% BSA and incubated for 1 h. The chamber was washed with 1% BSA, and OMVs (1:50 dilution) were added. The unbound OMVs were washed thoroughly with Tris buffer and subsequently imaged using a Nikon Ti inverted microscope, equipped with a 100× oil immersion objective. An LED light engine from Aura II, Lumencor was used to excite fluorescence, and a TRITC (chroma) filter set was utilized. A 2048 × 2048 pixel sCMOS camera (Orca Flash 4.0 v2, Hamamatsu) was used to capture all images. Using ImageJ, OMVs were counted over three 2048 × 2048 pixel frames (repeated 3 times) and data were normalized to the Anti-OmpA passivated OMV count. The data were analyzed using GraphPad Prism v 9.0.
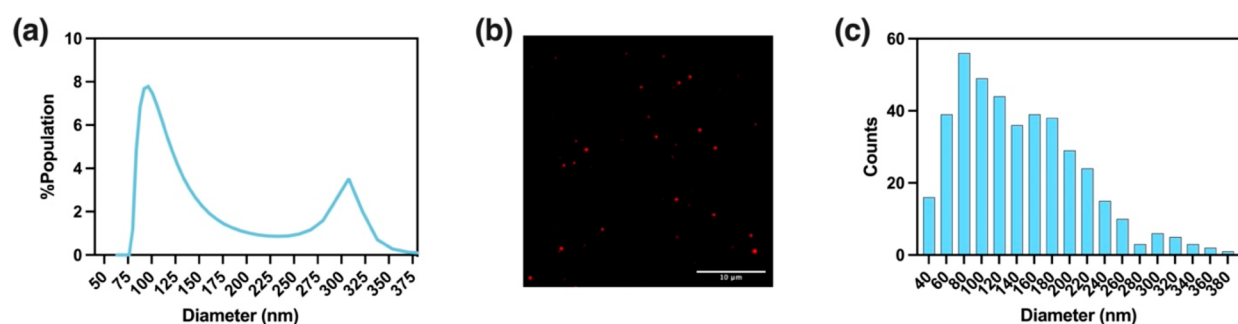
Figure 2. *A. actinomycetemcomitans* JP2 OMV characterization: (a) bimodal size distribution by DLS analysis, (b) integrated fluorescence intensity of DiI-labeled individual OMVs (scale bar: 10 μm), and (c) bimodal size distribution by fluorescence particle sizing analysis. A total of 416 OMVs were counted for JP2.

OMV Capture

Glass coverslips (cleaned with IPA and 2% SDS) were UV/ozone treated for 10 min (UV/Ozone ProCleaner Plus, BioForce Nanosciences) and passivated with 200 μg/mL of streptavidin to capture OMVs, prepared in 1% BSA. The coverslip was washed with 1% BSA, and OMVs (1:50 dilution) were added to the chamber and incubated for 1 h. Unbound OMVs were washed from the chamber, and bound OMVs were subsequently imaged using a Nikon Ti inverted microscope equipped with a 100× oil immersion objective. The LED light engine from the Aura II, Lumencor was used to excite fluorescence, and a Cy5 (Chroma) or TRITC (Chroma) filter set was utilized. A 2048 × 2048 pixel sCMOS camera (Orca Flash 4.0 v2, Hamamatsu) was used to capture all images. ImageJ was used to analyze the images and calculate the integrated intensity of the OMVs. The fluorescence intensity was converted to a size using the equations described below in the Results and Discussion section.

OMV Heterogeneity Analysis

Once the OMVs were imaged, a full-length anti-LtxA antibody was introduced to the chamber (1:1000 dilution). The anti-LtxA antibody was incubated for 1 h and subsequently washed with Tris buffer. Two μg/mL of secondary IgG with Alexa-488 (Abcam) was added to the chamber and incubated for 1 h. Excess antibody was washed, and the samples were imaged, as described previously. The FITC (Chroma) filter set was used to capture the antibody binding. Using ImageJ, the TRITC and FITC color channel were overlaid, and the x/y coordinates of the OMVs and antibody were analyzed to determine toxin-positive/negative OMVs. The toxin-positive and toxin-negative OMVs were separated into two categories, and their size distribution was plotted using GraphPad Prism v 9.0. To determine the toxin density present on the surface of the OMVs, the integrated intensity from the antibody was divided by the integrated intensity of the respective OMVs (I_t/I_v). The antibody surface passivation experiment procedure is outlined above.

Size Exclusion Chromatography of *A. actinomycetemcomitans* OMVs

Size exclusion chromatography (SEC) was used to separate OMVs by size; a 1.5 cm × 50 cm (bed volume 85 mL) was packed with Sephacryl S-1000 superfine resin (GE Healthcare, Chicago, IL, USA) and equilibrated with two bed volumes of PBS. A 2 mL OMV sample was loaded and eluted with PBS, and 1 mL fractions were collected. Fractions were analyzed for lipid and LtxA content, as described below.

The percentage of lipid in each SEC fraction was measured using the FM 4-64 dye (ThermoFisher Scientific, Waltham, MA). First, 50 μL of each fraction was incubated with FM 4-64 (0.1 mg/mL) for 15 s. Following incubation, the fluorescence of the sample was measured on a Tecan plate reader with an excitation wavelength of 515 nm and an emission wavelength of 640 nm. The fluorescence intensity of each fraction was divided by the summed intensities to calculate a percentage of total lipid in each fraction.

Western Blot and ELISA Analysis of OMV

The LtxA concentration in each SEC fraction was measured using ELISA. Fractions were incubated in a MaxiSorp Immuno 96-well plate (ThermoFisher Scientific) for 3 h, washed five times with ELISA wash buffer (25 M Tris, 150 mM sodium chloride, 0.1% fatty-acid free bovine serum albumin (BSA)), and then blocked in 1% BSA in the same buffer. The plate was then incubated with anti-LtxA antibody in 1% BSA/buffer overnight at 4 °C. Following five washes with ELISA wash buffer, the plate was incubated in goat antimouse horseradish peroxidase (GAM-HRP) at a 1:5000 ratio (SouthernBiotech, Birmingham, AL). Lastly, the plate was imaged using 1-Step Ultra TMB ELISA substrate solution (ThermoFisher Scientific) until the signal appeared; then, the reaction was stopped using 2 M sulfuric acid. The absorbance at 450 nm was measured on a Tecan plate reader. The resulting absorbance of each fraction was divided by the summed absorbances to calculate a percentage of total LtxA in each fraction.

LtxA content was also analyzed by Western blotting. Sodium dodecyl sulfate polyacrylamide gel electrophoresis (SDS-PAGE) was performed using 7.5% acrylamide gels. Western blotting for LtxA was accomplished by transferring the proteins to a nitrocellulose membrane overnight. The blots were washed three times in tris-buffered saline with 0.1% tween (TBST) and then blocked with blotto solution (5% dried milk in TBST) for 1 h. LtxA was then detected using a monoclonal anti-LtxA antibody overnight at 4 °C, followed by GAM-HRP for 1 h. The blot was imaged using SuperSignal West Dura substrate (ThermoFisher). To measure the amount of outer membrane protein-A (OmpA) in each fraction, a similar procedure was used, with the anti-Gram-negative OmpA antibody (111228, Antibody Research Corporation, St. Charles, MO) at a final concentration of 0.24 μg/mL, followed by goat antirabbit horseradish peroxidase (GAR-HRP, SouthernBiotech). Densitometry analysis on the blots was accomplished using ImageJ.

■ RESULTS AND DISCUSSION

OMV Size Determination Using Fluorescence Microscopy

As a study model, we utilized *Aggregatibacter actinomycetemcomitans*, an oral bacterium associated with aggressive forms of periodontitis.[47] As part of its virulence, *A. actinomycetemcomitans* produces leukotoxin A (LtxA), which targets leukocytes.[33,48] *A. actinomycetemcomitans* secretes LtxA in two forms: water-soluble free LtxA and LtxA attached on the surface of OMVs.[33,41] Interestingly, *A. actinomycetemcomitans* produces a bimodal size distribution of OMVs, where a predominant population of ~100 nm in diameter is observed along with a minor population of ~350 nm in diameter.[41,49] Here, we aimed to determine how the toxin was distributed among the OMV populations.

First, we aimed to analyze the diameter of OMVs produced by two *A. actinomycetemcomitans* strains, JP2 and AA1704.

While JP2 secretes high levels of leukotoxin, AA1704 is an isogenic mutant of JP2 that is deficient in LtxA production.[50−52] Dynamic light scattering (DLS) analysis reveals that both strains produce a heterogeneous population of OMVs, as indicated by the bimodal size distribution observed (Figure 2a and Figure S1). Our next objective was to determine the size of OMVs using single-particle fluorescence sizing. Labeling OMVs with fluorescent lumen dyes is one possible approach, but it presents challenges such as incomplete labeling of OMVs and uneven packing of the dye. To obtain an accurate representation of size using fluorescence microscopy, we utilized a lipophilic membrane dye (DiI) that incorporates itself into the OMV membrane; thus, the integrated fluorescence intensity of each particle provides a reliable representation of the surface area. After exposing OMVs to biotin ap-PE, which incorporates into the membrane due to its hydrophobic nature, we captured them on streptavidin- and BSA-passivated glass (Figure 2b). We opted to employ the biotin−streptavidin immobilization approach, as it offers a high affinity between biotin−streptavidin, guaranteeing firm immobilization of OMVs throughout the sizing and heterogeneity experiments.[53,54] As an alternate, an antibody could also be used to capture the OMVs;[55] however, this would require the prior knowledge of the presence of certain proteins. We specifically utilized biotin Cap-PE, a membrane-specific label, to label our OMVs, which guarantees the unbiased capture of all OMVs regardless of their size or the presence of specific surface markers.

To achieve high-throughput fluorescence intensity measurement, we implemented automation through ImageJ's particle analysis method. It is crucial to highlight that biological samples can exhibit aggregation tendencies. To mitigate this, we meticulously ensured that only individual OMVs were considered in the analysis, utilizing the circularity option. Given that a single OMV should ideally possess perfect circularity (a circularity value of 1), we permitted a slight deviation, ranging from 1 to 0.7.[46] This flexibility accommodates possible irregularities arising from the biological nature of the samples, all while rigorously maintaining control to prevent the inclusion of aggregated entities including membrane dye aggregation. We preceded by measuring the fluorescence intensity of the captured OMVs and observed that each OMV displayed a unique integrated fluorescence intensity (Figure S3), which is proportional to its surface area, and thus can be used to determine the size distribution of the vesicle population.

To convert the intensity distribution to a diameter distribution, the following mathematical conversions were used, building upon the approach pioneered by Stamou and co-workers.[46] The surface area of the OMVs (SA_{OMVs}) is directly proportional to the measured integrated fluorescence intensity (I_M), meaning that larger OMVs will exhibit larger integrated intensities (eq 1). By assuming that OMVs are spherical, we were able to solve for their surface area (eq 2). Equations 1 and 2 can be combined to relate the intensity observed to the radius (r) using a correlation factor k (eq 3). This correlation factor k relates the intensity of a single vesicle to its radius in nm, and it is dependent on factors such as the photophysical properties of the fluorophore and the signal detection efficiency. The value of k can be calculated using eq 4, where r_{mean} is the mean radius determined using other sizing methods. In this study, DLS was used to calculate the

$r_{mean(DLS)}$), and the radius of each OMV can be calculated using eq 5; then, a radius or diameter distribution was generated.

$$SA_{OMVs} \propto I_M \tag{1}$$

$$SA_{OMVs} = 4\pi r^2 \tag{2}$$

$$r = k\sqrt{I_M} \tag{3}$$

$$k = \frac{r_{mean(DLS)}}{\sqrt{I_M}_{(Mean)}} \tag{4}$$

$$r = \frac{r_{mean(DLS)}}{\sqrt{I_M}_{(Mean)}} \times \sqrt{I_M} \tag{5}$$

The fluorescence-based size distribution was generated using the fluorescence intensity distribution, and the analysis revealed the presence of two populations of OMVs, one with a diameter of roughly 100 nm and the other with a diameter of around 300 nm (Figure 2c). The results obtained from the fluorescence intensity analysis were consistent with our previous findings from DLS showing a diameter of roughly 100 nm and the other with a diameter of around 300 nm.

We applied a similar approach to analyze OMVs generated by the *A. actinomycetemcomitans* 1704 strain, where we analyzed 416 individual OMVs to generate the size distribution. The outcome revealed a similar bimodal size distribution, with a predominant population centered around 120 nm and a smaller population at approximately 300 nm (Figure S4).

Previously, the fluorescence single-particle sizing has primarily been utilized for synthetic particles.[46,56] Therefore, there was a possibility that the bimodal size observed in *A. actinomycetemcomitans* OMVs may not be an accurate representation of their size but rather a result of biological factors such as aggregation. To confirm that the bimodal size distribution of *A. actinomycetemcomitans* OMVs truly reflected their size heterogeneity, we also analyzed *E. coli* OMVs, which have a unimodal size distribution (Figure S5). Both *E. coli* OMVs and *A. actinomycetemcomitans* OMVs were labeled with the same membrane fluorescent dye (DiI) and biotinylated to ensure a fair comparison of their integrated intensity. The results showed that *E. coli* OMVs had a unimodal integrated intensity distribution which results in a unimodal size distribution, confirming that the bimodal distribution observed in *A. actinomycetemcomitans* OMVs was due to their heterogeneous size population (Figure S5). The integrated intensity distribution of *E. coli* OMVs displayed a distinct shift to lower values, indicating the presence of OMVs that are smaller than those produced by *A. actinomycetemcomitans*; the majority of these OMVs had a square root integrated intensity of approximately 300 i.u. This observation suggests a correlation between the diameter of the OMVs and their intensity, as the smaller size of *E. coli* OMVs likely results in lower integrated intensity. In contrast, *A. actinomycetemcomitans* OMVs displayed maxima at higher integrated intensities of 600 and 2250 i.u., suggesting a larger and heterogeneous diameter for these OMVs (Figure S5). These results highlight the effectiveness of fluorescence microscopy in accurately determining the size distribution of both heterogeneous and homogeneous size populations of OMVs.

Surface Toxin Discrepancy in *A. actinomycetemcomitans* OMVs

Once the size of the OMVs was determined, we investigated the potential for toxin variation on the surface of individual *A. actinomycetemcomitans* OMVs. To examine this possibility, we conducted an experiment with a glass surface coated with an anti-LtxA antibody (Figure 3a). The OMVs were then exposed
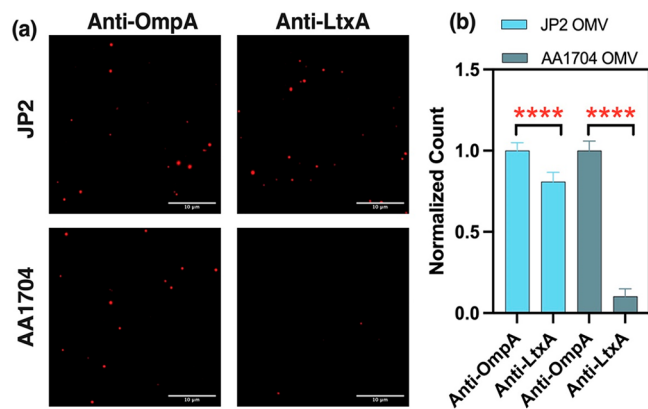
Figure 3. Analysis of OMV surface proteins: (a) Micrographs of OMVs captured on glass passivated with anti-LtxA antibody, compared to ubiquitous anti-OmpA protein passivation. (b) The normalized counts of OMVs show significantly lower binding of JP2 OMVs to the anti-LtxA antibody compared to the negative control, AA1704 OMVs. ****A *p*-value of less than 0.0001 indicates a significant difference in the presence of LtxA on the OMV surface.

to the antibody-coated glass and counted based on the number of OMVs that bound in three 2048 × 2048 pixel areas. A control experiment was performed targeting outer membrane protein A (OmpA), which is commonly found on OMV surfaces,[28,33,57] to normalize the count of OMVs (Figure 3b). Our results indicated significantly fewer JP2 OMVs bound to the anti-LtxA coated surface, suggesting that LtxA is present on only a subset of these OMVs (Figure 3b). Additionally, a control experiment was performed with the LtxA deletion mutant (AA1704), and no significant binding to the anti-LtxA was observed, further verifying the specificity of the antibody toward the toxin (Figure 3b).

To further investigate the observed enrichment of toxin on a subpopulation of OMVs, we biotinylated the OMVs and immobilized them on a streptavidin surface. We then exposed the OMVs to the anti-LtxA antibody and added a secondary antibody conjugated with a fluorophore to mark the presence of the toxin. We combined the channel displaying OMV membrane fluorescence and the antibody channel to visualize the colocalization between the two. This approach allowed us to determine the distribution of LtxA on the OMV surface and determine any size-based heterogeneities. Our results showed that, while some JP2 OMVs were positive for the toxin, others lacked it (Figure 4a). To serve as a negative control, we also evaluated the binding of the secondary antibody in the absence of the primary antibody, demonstrating the specificity of the observed signal (Figure S6). Additionally, we also tested OMVs for the presence of outer membrane protein A (OmpA), which is present ubiquitously on the OMV surface,[28,33,57] and observed the vast majority of the OMVs had the antibody bind to the surface (Figure 4b). Given the homogeneous binding of anti-OmpA, our primary focus shifted toward investigating discrepancies in LtxA interactions. As an
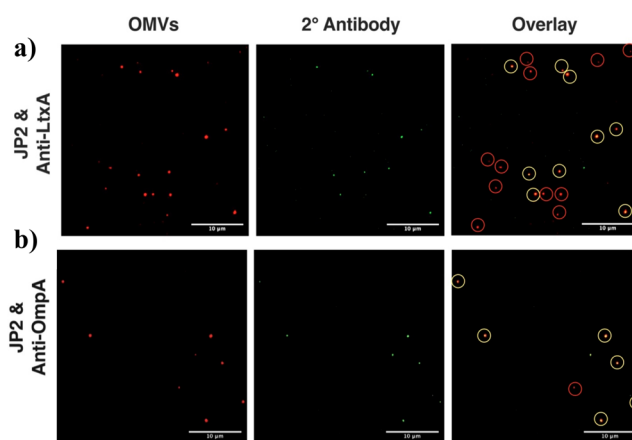
Figure 4. Surface protein analysis of *A. actinomycetemcomitans* OMVs: (a) OMVs from the JP2 strain were analyzed for the presence of LtxA. The fluorescence micrograph shows only a few OMVs with positive staining for LtxA, indicating that not all OMVs carry this virulence factor. (b) Positive control: OMVs were analyzed for ubiquitous OmpA. Yellow circles indicate the colocalized antibody and the OMVs, while red circles highlight the OMVs lacking LtxA or OmpA.

additional negative control, we assayed AA1704 OMVs (which do not express LtxA) for LtxA and did not observe any antibody binding (Figure S7). Our results confirm that our platform is capable of detecting individual OMV heterogeneity, including size-based heterogeneities as well as compositional heterogeneities such as the presence of the toxin or proteins, as demonstrated by the binding observed only in OMVs containing the toxin.

Size-Dependent Toxin Sorting in *A. actinomycetemcomitans* OMV

To determine if the discrepancies in LtxA antibody binding with JP2 OMVs were size-based, we categorized the OMVs into two groups based on the presence of LtxA, toxin-positive and toxin-negative, and then analyzed their size distributions. Our findings indicate that LtxA was primarily present in larger OMVs, with only the smallest diameter OMVs devoid of the toxin. The significance of single-OMV analysis was highlighted by our noteworthy findings: no LtxA-negative OMVs were found to have a diameter greater than 220 nm, and no LtxA-positive OMVs were found to have a diameter smaller than 60 nm (Figure 5a). This analysis enables the detection of biomolecular distributions on OMVs that are often obscured by traditional ensemble assays. Furthermore, we investigated the correlation between toxin presence or absence and OMV diameter, and our observations revealed in the range of 140 nm that there was an even split of LtxA-positive and -negative OMVs, indicating a heterogeneous population. Our examination of overall OMV positivity and negativity for toxins in relation to diameter revealed a proportional increase in toxin-positive OMVs and a decrease in toxin-negative OMVs as the OMV size increased (Figure 5b).

After observing the presence of LtxA in larger OMVs, we aimed to determine if there was a correlation between the size of the OMVs and the density of the toxin. To do this, we analyzed the toxin density where we divided the integrated intensity of the LtxA antibody staining by the integrated intensity of the vesicle membrane (Figure 5c). We found that the size of OMVs and the density of the toxin were not significantly correlated, as supported by a Pearson correlation
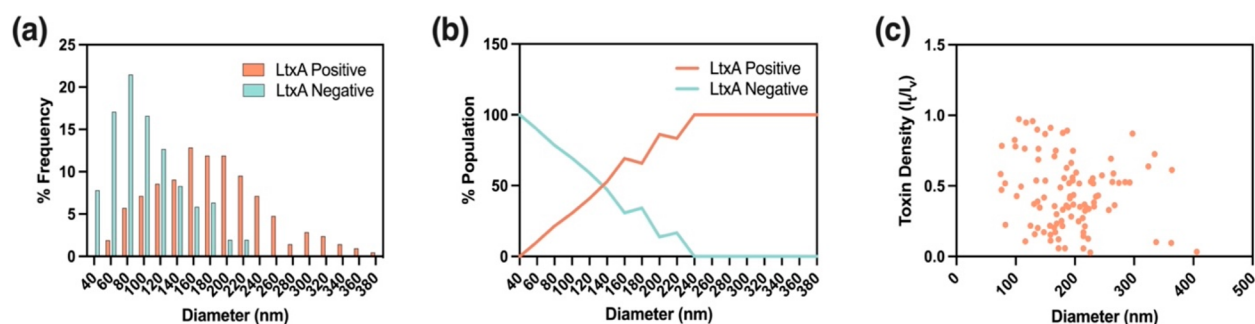
Figure 5. Size-based toxin heterogeneity analysis: (a) Fluorescently labeled OMVs were analyzed for the presence of LtxA toxin. No LtxA-negative OMVs were found to have a diameter greater than 220 nm, while no LtxA-positive OMVs had a diameter smaller than 60 nm. (b) Fraction LtxA-positive and -negative as a function of OMV diameter. (c) Toxin density plotted against vesicle diameter.
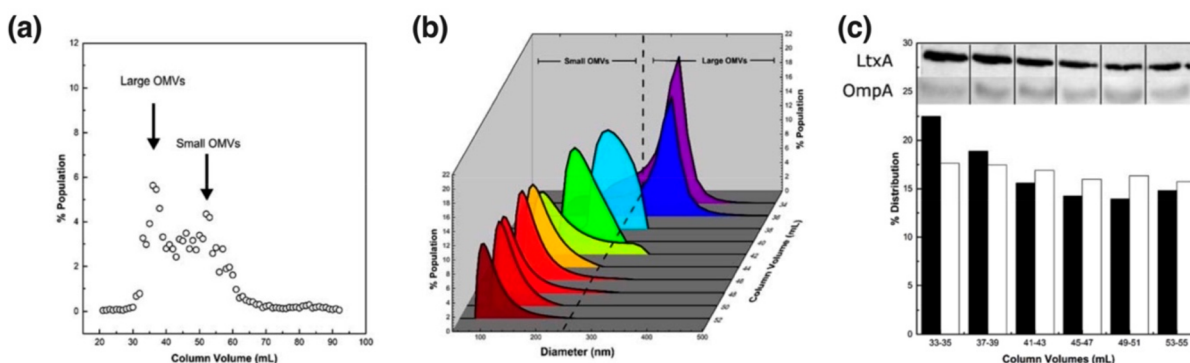
Figure 6. Analysis of OMVs separated based on their size: (a) OMVs were separated by SEC. The fluorescence of a lipid probe, FM 4-64 (open circles), was used to identify fractions containing OMVs. (b) SEC fractions were analyzed using DLS to determine the size distribution of OMVs. (c) Western blot analysis of LtxA and OmpA in each fraction, normalized to their respective lipid content.

coefficient (r) of −0.168 and a p-value of 0.906. This suggests that the larger OMVs, which have up to 10 times more surface area than the smaller OMVs, do not necessarily have more LtxA present per vesicle. These results highlight the importance of further investigation into the mechanisms controlling toxin sorting and distribution within OMVs.

We validated our toxin distribution analysis of OMVs using an ELISA and Western blot assay. To investigate size-based heterogeneity, it was crucial to separate the OMVs based on size prior to the Western blot analysis. An ultrafine Sepharose S1000 column has been used previously for size-based OMV separation, which is a simpler alternative to traditional methods like density gradient centrifugation.[29] We aimed to utilize this method to separate *A. actinomycetemcomitans* OMVs into fractions based on their size. Our analysis of chromatographic fractions confirmed the presence of two populations of OMVs, eluting in different volumes (Figure 6a). DLS measurements showed that larger OMVs (over 250 nm) were found in the 34−36 mL fractions, while smaller OMVs (under 250 nm) were found in the 44−52 mL fractions (Figure 6b). Next, the OMV fractions were analyzed to determine the presence of LtxA. The results from ELISA showed that much of the LtxA was found in fractions containing the larger OMVs (Figure S8), in agreement with the single-particle fluorescence analysis. To address the potential of the toxin being observed in larger OMVs due to a greater surface area, we performed Western blot on SEC fractions that were normalized by their total lipid concentration. The results showed that the larger OMVs (33−35 mL) had more LtxA, and the fractions containing smaller OMVs had less (Figure 6c). As a positive control, the presence of

OmpA in the OMV fractions was also detected by Western blotting, and the results showed that OmpA was present in all fractions, while a notable trend of increasing LtxA level with OMV size was observed (Figure 6c). These results further confirm the validity of our method.

■ CONCLUSIONS

OMVs play a vital role in various processes, including cell-to-cell communication, horizontal gene transfer, and pathogenesis. Despite their significance, the heterogeneous size and composition of OMVs pose challenges in understanding their functionality and interaction with target cells. Conventional OMV analysis assays, which rely on population measurements, ignore variations between individual OMVs. Although single-OMV analysis methods exist, they can often be limited in their scope.

Our study presents an approach using fluorescence-based particle sizing to uncover size-based heterogeneities in bacterial OMVs. This method enables simultaneous detection of size and surface toxin/protein content on individual OMVs, providing a comprehensive characterization of these complex nanoparticles. Our results demonstrate the versatility and effectiveness of our method in accurately determining the size distribution and heterogeneity of OMVs. We utilized fluorescence microscopy to analyze heterogeneous populations of OMVs produced by the oral bacterium *A. actinomycetemcomitans*. The results from our study provide new insights into the size distribution of *A. actinomycetemcomitans* OMVs and reveal the presence of two populations of OMVs, one with a size of roughly 100 nm and the other with a

diameter of around 300 nm. Furthermore, our single-particle analysis allowed us to discover that no LtxA-negative OMVs were found to have a diameter greater than 220 nm and no LtxA-positive OMVs were found to have a diameter smaller than 60 nm. These results highlight the significance of single-OMV analysis as it enables the detection of nanoscale biomolecular distribution on OMVs that are masked by traditional ensemble assays.

Previous studies have mainly reported unimodal size distributions for clinically significant OMVs, including those released by *Acinetobacter baumannii*, *Pseudomonas aeruginosa*, *E. coli*, and *Enterobacter cloacae*.[34,58−60] It is important to note that, although most OMVs exhibit a unimodal size distribution, they still have a wide size range exhibiting a heterogeneous population of size. Our results highlight that smaller-diameter *A. actinomycetemcomitans* OMVs, ranging from 75 to 175 nm, contained a mixture of toxin-positive and toxin-negative vesicles suggesting that there can be substantial differences within a unimodal size distribution OMV, leading to function differences as previously seen with the bimodal OMVs of *H. pylori*.[24]

In conclusion, our platform is unique in its approach as it does not require OMVs to be separated and is noninvasive, utilizing a general-purpose microscope instead of specialized equipment. Our study highlights the versatility and effectiveness of our method in accurately determining the size distribution and heterogeneity of OMVs and offers a more comprehensive and advanced approach to studying OMVs.

◼ ASSOCIATED CONTENT

ⓢ Supporting Information

The Supporting Information is available free of charge at https://pubs.acs.org/doi/10.1021/cbmi.4c00014.

> Dynamic light scattering analysis of OMVs, scanning electron micrographs of OMVs, and additional fluorescence images of individual OMVs (PDF)

◼ AUTHOR INFORMATION

Corresponding Author

Nathan J. Wittenberg − *Department of Chemistry, Lehigh University, Bethlehem, Pennsylvania 18015, United States;* ⓞ orcid.org/0000-0001-9196-1867; Email: njw@lehigh.edu

Authors

Aarshi N. Singh − *Department of Chemistry, Lehigh University, Bethlehem, Pennsylvania 18015, United States;* ⓞ orcid.org/0000-0002-5888-4449

Justin B Nice − *Department of Chemical and Biomolecular Engineering, Lehigh University, Bethlehem, Pennsylvania 18015, United States*

Meishan Wu − *Department of Chemical and Biomolecular Engineering, Lehigh University, Bethlehem, Pennsylvania 18015, United States*

Angela C. Brown − *Department of Chemical and Biomolecular Engineering, Lehigh University, Bethlehem, Pennsylvania 18015, United States;* ⓞ orcid.org/0000-0003-1038-8216

Complete contact information is available at:
https://pubs.acs.org/10.1021/cbmi.4c00014

Notes

The authors declare no competing financial interest.

◼ REFERENCES

(1) Schwechheimer, C.; Kuehn, M. J. Outer-Membrane Vesicles from Gram-Negative Bacteria: Biogenesis and Functions. *Nat. Rev. Microbiol.* **2015**, *13* (10), 605−619.

(2) Kulp, A.; Kuehn, M. J. Biological Functions and Biogenesis of Secreted Bacterial Outer Membrane Vesicles. *Annu. Rev. Microbiol.* **2010**, *64* (1), 163−184.

(3) Jan, A. T. Outer Membrane Vesicles (OMVs) of Gram-Negative Bacteria: A Perspective Update. *Front. Microbiol.* **2017**, *8*, 1053.

(4) Deatherage, B. L.; Cookson, B. T. Membrane Vesicle Release in Bacteria, Eukaryotes, and Archaea: A Conserved yet Underappreciated Aspect of Microbial Life. *Infect. Immun.* **2012**, *80* (6), 1948−1957.

(5) Rueter, C.; Bielaszewska, M. Secretion and Delivery of Intestinal Pathogenic Escherichia Coli Virulence Factors via Outer Membrane Vesicles. *Front. Cell. Infect. Microbiol.* **2020**, *10*, 91.

(6) Chowdhury, C.; Jagannadham, M. V. Virulence Factors Are Released in Association with Outer Membrane Vesicles of Pseudomonas Syringae Pv. Tomato T1 during Normal Growth. *Biochimica et Biophysica Acta (BBA) - Proteins and Proteomics* **2013**, *1834* (1), 231−239.

(7) Chatterjee, D.; Chaudhuri, K. Association of Cholera Toxin with *Vibrio Cholerae* Outer Membrane Vesicles Which Are Internalized by Human Intestinal Epithelial Cells. *FEBS Lett.* **2011**, *585* (9), 1357−1362.

(8) Bielaszewska, M.; Rüter, C.; Kunsmann, L.; Greune, L.; Bauwens, A.; Zhang, W.; Kuczius, T.; Kim, K. S.; Mellmann, A.; Schmidt, M. A.; Karch, H. Enterohemorrhagic Escherichia Coli Hemolysin Employs Outer Membrane Vesicles to Target Mitochondria and Cause Endothelial and Epithelial Apoptosis. *PLoS Pathog* **2013**, *9* (12), No. e1003797.

(9) Holst, J.; Martin, D.; Arnold, R.; Huergo, C. C.; Oster, P.; O'Hallahan, J.; Rosenqvist, E. Properties and Clinical Performance of Vaccines Containing Outer Membrane Vesicles from Neisseria Meningitidis. *Vaccine* **2009**, *27*, B3−B12.

(10) Balhuizen, M. D.; Veldhuizen, E. J. A.; Haagsman, H. P. Outer Membrane Vesicle Induction and Isolation for Vaccine Development. *Front. Microbiol.* **2021**, *12*, No. 629090.

(11) Wang, G.; Narayana, J. L.; Mishra, B.; Zhang, Y.; Wang, F.; Wang, C.; Zarena, D.; Lushnikova, T.; Wang, X. Design of Antimicrobial Peptides: Progress Made with Human Cathelicidin LL-37. In *Antimicrobial Peptides*; Matsuzaki, K., Ed.; Advances in Experimental Medicine and Biology; Springer Singapore: Singapore, 2019; Vol. *1117*, pp 215−240. DOI: 10.1007/978-981-13-3588-4_12.

(12) Gujrati, V.; Kim, S.; Kim, S.-H.; Min, J. J.; Choy, H. E.; Kim, S. C.; Jon, S. Bioengineered Bacterial Outer Membrane Vesicles as Cell-Specific Drug-Delivery Vehicles for Cancer Therapy. *ACS Nano* **2014**, *8* (2), 1525−1537.

(13) Kuerban, K.; Gao, X.; Zhang, H.; Liu, J.; Dong, M.; Wu, L.; Ye, R.; Feng, M.; Ye, L. Doxorubicin-Loaded Bacterial Outer-Membrane Vesicles Exert Enhanced Anti-Tumor Efficacy in Non-Small-Cell Lung Cancer. *Acta Pharmaceutica Sinica B* **2020**, *10* (8), 1534−1548.

(14) Kim, O. Y.; Park, H. T.; Dinh, N. T. H.; Choi, S. J.; Lee, J.; Kim, J. H.; Lee, S.-W.; Gho, Y. S. Bacterial Outer Membrane Vesicles Suppress Tumor by Interferon-γ-Mediated Antitumor Response. *Nat. Commun.* **2017**, *8* (1), 626.

(15) Jalalifar, S.; Morovati Khamsi, H.; Hosseini-Fard, S. R.; Karampoor, S.; Bajelan, B.; Irajian, G.; Mirzaei, R. Emerging Role of Microbiota Derived Outer Membrane Vesicles to Preventive, Therapeutic and Diagnostic Proposes. *Infect Agents Cancer* **2023**, *18* (1), 3.

(16) Huang, H. W.; Charron, N. E. Understanding Membrane-Active Antimicrobial Peptides. *Q. Rev. Biophys.* **2017**, *50*, e10.

(17) Collins, S. M.; Brown, A. C. Bacterial Outer Membrane Vesicles as Antibiotic Delivery Vehicles. *Front. Immunol.* **2021**, *12*, No. 733064.

(18) Zavan, L.; Bitto, N. J.; Johnston, E. L.; Greening, D. W.; Kaparakis-Liaskos, M. *Helicobacter Pylori* Growth Stage Determines the Size, Protein Composition, and Preferential Cargo Packaging of Outer Membrane Vesicles. *Proteomics* **2019**, *19*, 1800209.

(19) Balsalobre, C.; Silvan, J. M.; Berglund, S.; Mizunoe, Y.; Uhlin, B. E.; Wai, S. N. Release of the Type I Secreted Alpha-Haemolysin via Outer Membrane Vesicles from Escherichia Coli. *Mol. Microbiol.* **2006**, *59* (1), 99−112.

(20) Zingl, F. G.; Thapa, H. B.; Scharf, M.; Kohl, P.; Müller, A. M.; Schild, S. Outer Membrane Vesicles of Vibrio Cholerae Protect and Deliver Active Cholera Toxin to Host Cells via Porin-Dependent Uptake. *mBio* **2021**, *12* (3), No. e00534-21.

(21) O'Donoghue, E. J.; Krachler, A. M. Mechanisms of Outer Membrane Vesicle Entry into Host Cells: MicroReview - OMV Entry into Host Cells. *Cellular Microbiology* **2016**, *18* (11), 1508−1517.

(22) Parker, H.; Chitcholtan, K.; Hampton, M. B.; Keenan, J. I. Uptake of *Helicobacter Pylori* Outer Membrane Vesicles by Gastric Epithelial Cells. *Infect. Immun.* **2010**, *78* (12), 5054−5061.

(23) Furuta, N.; Tsuda, K.; Omori, H.; Yoshimori, T.; Yoshimura, F.; Amano, A. *Porphyromonas Gingivalis* Outer Membrane Vesicles Enter Human Epithelial Cells via an Endocytic Pathway and Are Sorted to Lysosomal Compartments. *Infect. Immun.* **2009**, *77* (10), 4187−4196.

(24) Turner, L.; Bitto, N. J.; Steer, D. L.; Lo, C.; D'Costa, K.; Ramm, G.; Shambrook, M.; Hill, A. F.; Ferrero, R. L.; Kaparakis-Liaskos, M. Helicobacter Pylori Outer Membrane Vesicle Size Determines Their Mechanisms of Host Cell Entry and Protein Content. *Front. Immunol.* **2018**, *9*, 1466.

(25) Price, N. L.; Goyette-Desjardins, G.; Nothaft, H.; Valguarnera, E.; Szymanski, C. M.; Segura, M.; Feldman, M. F. Glycoengineered Outer Membrane Vesicles: A Novel Platform for Bacterial Vaccines. *Sci. Rep* **2016**, *6* (1), 24931.

(26) Jin, J. S.; Kwon, S.-O.; Moon, D. C.; Gurung, M.; Lee, J. H.; Kim, S. I.; Lee, J. C. Acinetobacter Baumannii Secretes Cytotoxic Outer Membrane Protein A via Outer Membrane Vesicles. *PLoS One* **2011**, *6* (2), No. e17027.

(27) Bernadac, A.; Gavioli, M.; Lazzaroni, J.-C.; Raina, S.; Lloubès, R. *Escherichia Coli Tol-Pal* Mutants Form Outer Membrane Vesicles. *J. Bacteriol.* **1998**, *180* (18), 4872−4878.

(28) Rompikuntal, P. K.; Thay, B.; Khan, M. K.; Alanko, J.; Penttinen, A.-M.; Asikainen, S.; Wai, S. N.; Oscarsson, J. Perinuclear Localization of Internalized Outer Membrane Vesicles Carrying Active Cytolethal Distending Toxin from Aggregatibacter Actino-mycetemcomitans. *Infect. Immun.* **2012**, *80* (1), 31−42.

(29) Collins, S. M.; Nice, J. B.; Chang, E. H.; Brown, A. C. Size Exclusion Chromatography to Analyze Bacterial Outer Membrane Vesicle Heterogeneity. *JoVE* **2021**, *169*, 62429.

(30) Dick, L. W., Jr; Mehl, J. T.; Loughney, J. W.; Mach, A.; Rustandi, R. R.; Ha, S.; Zhang, L.; Przysiecki, C. T.; Dieter, L.; Hoang, V. M. Label-Free Quantitative Mass Spectrometry for Analysis of Protein Antigens in a Meningococcal Group B Outer Membrane Vesicle Vaccine. *Human Vaccines & Immunotherapeutics* **2015**, *11* (6), 1518−1525.

(31) Uli, L.; Castellanos-Serra, L.; Betancourt, L.; Domínguez, F.; Barberá, R.; Sotolongo, F.; Guillén, G.; Pajón Feyt, R. Outer Membrane Vesicles of the VA-MENGOC-BC® Vaccine against Serogroup Bof Neisseria Meningitidis: Analysis of Protein Compo-nents by Two-Dimensional Gel Electrophoresis and Mass Spectrom-etry. *Proteomics* **2006**, *6* (11), 3389−3399.

(32) Turkina, M. V.; Olofsson, A.; Magnusson, K.-E.; Arnqvist, A.; Vikström, E. Helicobacter Pylori Vesicles Carrying CagA Localize in the Vicinity of Cell−Cell Contacts and Induce Histone H1 Binding to ATP in Epithelial Cells. *FEMS Microbiology Letters* **2015**, *362* (11), No. fnv076.

(33) Kieselbach, T.; Zijnge, V.; Granström, E.; Oscarsson, J. Proteomics of Aggregatibacter Actinomycetemcomitans Outer Mem-brane Vesicles. *PLoS One* **2015**, *10* (9), No. e0138591.

(34) Bhar, S.; Edelmann, M. J.; Jones, M. K. Characterization and Proteomic Analysis of Outer Membrane Vesicles from a Commensal Microbe, Enterobacter Cloacae. *Journal of Proteomics* **2021**, *231*, No. 103994.

(35) Antenucci, F.; Arak, H.; Gao, J.; Allahgadry, T.; Thøfner, I.; Bojesen, A. M. Hydrostatic Filtration Enables Large-Scale Production of Outer Membrane Vesicles That Effectively Protect Chickens against Gallibacterium Anatis. *Vaccines* **2020**, *8* (1), 40.

(36) Roier, S.; Zingl, F. G.; Cakar, F.; Durakovic, S.; Kohl, P.; Eichmann, T. O.; Klug, L.; Gadermaier, B.; Weinzerl, K.; Prassl, R.; Lass, A.; Daum, G.; Reidl, J.; Feldman, M. F.; Schild, S. A Novel Mechanism for the Biogenesis of Outer Membrane Vesicles in Gram-Negative Bacteria. *Nat. Commun.* **2016**, *7* (1), 10515.

(37) Gerritzen, M. J. H.; Martens, D. E.; Wijffels, R. H.; Stork, M. High Throughput Nanoparticle Tracking Analysis for Monitoring Outer Membrane Vesicle Production. *J. of Extracellular Vesicle* **2017**, *6* (1), 1333883.

(38) Zhang, L.; Zhao, S.; Zhang, J.; Sun, Y.; Xie, Y.; Liu, Y.; Ma, C.; Jiang, B.; Liao, X.; Li, W.; Cheng, X.; Wang, Z. Proteomic Analysis of Vesicle-Producing Pseudomonas Aeruginosa PAO1 Exposed to X-Ray Irradiation. *Front. Microbiol.* **2020**, *11*, No. 558233.

(39) Reimer, S. L.; Beniac, D. R.; Hiebert, S. L.; Booth, T. F.; Chong, P. M.; Westmacott, G. R.; Zhanel, G. G.; Bay, D. C. Comparative Analysis of Outer Membrane Vesicle Isolation Methods With an Escherichia Coli tolA Mutant Reveals a Hypervesiculating Phenotype With Outer-Inner Membrane Vesicle Content. *Front. Microbiol.* **2021**, *12*, No. 628801.

(40) Cecil, J. D.; O'Brien-Simpson, N. M.; Lenzo, J. C.; Holden, J. A.; Singleton, W.; Perez-Gonzalez, A.; Mansell, A.; Reynolds, E. C. Outer Membrane Vesicles Prime and Activate Macrophage Inflammasomes and Cytokine Secretion In Vitro and In Vivo. *Front. Immunol.* **2017**, *8*, 1017.

(41) Nice, J.; Balashova, N.; Kachlany, S.; Koufos, E.; Krueger, E.; Lally, E.; Brown, A. Aggregatibacter Actinomycetemcomitans Leukotoxin Is Delivered to Host Cells in an LFA-1-Indepdendent Manner When Associated with Outer Membrane Vesicles. *Toxins* **2018**, *10* (10), 414.

(42) Farrugia, C.; Stafford, G. P.; Murdoch, C. *Porphyromonas Gingivalis* Outer Membrane Vesicles Increase Vascular Permeability. *J. Dent Res.* **2020**, *99* (13), 1494−1501.

(43) Kadurugamuwa, J. L.; Beveridge, T. J. Virulence Factors Are Released from Pseudomonas Aeruginosa in Association with Membrane Vesicles during Normal Growth and Exposure to Gentamicin: A Novel Mechanism of Enzyme Secretion. *J. Bacteriol.* **1995**, *177* (14), 3998−4008.

(44) Li, Y.; Ma, X.; Yue, Y.; Zhang, K.; Cheng, K.; Feng, Q.; Ma, N.; Liang, J.; Zhang, T.; Zhang, L.; Chen, Z.; Wang, X.; Ren, L.; Zhao, X.; Nie, G. Rapid Surface Display of mRNA Antigens by Bacteria-Derived Outer Membrane Vesicles for a Personalized Tumor Vaccine. *Adv. Mater.* **2022**, *34* (20), 2109984.

(45) Zhang, Y.; Chen, Y.; Lo, C.; Zhuang, J.; Angsantikul, P.; Zhang, Q.; Wei, X.; Zhou, Z.; Obonyo, M.; Fang, R. H.; Gao, W.; Zhang, L. Inhibition of Pathogen Adhesion by Bacterial Outer Membrane-Coated Nanoparticles. *Angew. Chem., Int. Ed.* **2019**, *58* (33), 11404−11408.

(46) Lohr, C.; Kunding, A. H.; Bhatia, V. K.; Stamou, D. Constructing Size Distributions of Liposomes from Single-Object Fluorescence Measurements. *In Methods in Enzymology; Elsevier* **2009**, *465*, 143−160.

(47) Fine, D. H.; Patil, A. G.; Velusamy, S. K. Aggregatibacter Actinomycetemcomitans (Aa) Under the Radar: Myths and

Misunderstandings of Aa and Its Role in Aggressive Periodontitis. *Front. Immunol.* **2019**, *10*, 728.

(48) Johansson, A. Aggregatibacter Actinomycetemcomitans Leukotoxin: A Powerful Tool with Capacity to Cause Imbalance in the Host Inflammatory Response. *Toxins* **2011**, *3* (3), 242−259.

(49) Nice, J. B.; Collins, S. M.; Agro, S. M. J.; Sinani, A.; Moros, S. D.; Pasch, L. M.; Brown, A. C. Heterogeneity of Size and Toxin Distribution in Aggregatibacter Actinomycetemcomitans Outer Membrane Vesicles. *Toxins* **2024**, *16* (3), 138.

(50) Balashova, N. V.; Crosby, J. A.; Al Ghofaily, L.; Kachlany, S. C. Leukotoxin Confers Beta-Hemolytic Activity to *Actinobacillus Actinomycetemcomitans*. *Infect. Immun.* **2006**, *74* (4), 2015−2021.

(51) Brogan, J. M.; Lally, E. T.; Poulsen, K.; Kilian, M.; Demuth, D. R. Regulation of Actinobacillus Actinomycetemcomitans Leukotoxin Expression: Analysis of the Promoter Regions of Leukotoxic and Minimally Leukotoxic Strains. *Infect. Immun.* **1994**, *62* (2), 501−508.

(52) Haubek, D.; Poulsen, K.; Westergaard, J.; Dahlèn, G.; Kilian, M. Highly Toxic Clone of Actinobacillus Actinomycetemcomitans in Geographically Widespread Cases of Juvenile Periodontitis in Adolescents of African Origin. *J. Clin Microbiol* **1996**, *34* (6), 1576−1578.

(53) Lee, K.; Fraser, K.; Ghaddar, B.; Yang, K.; Kim, E.; Balaj, L.; Chiocca, E. A.; Breakefield, X. O.; Lee, H.; Weissleder, R. Multiplexed Profiling of Single Extracellular Vesicles. *ACS Nano* **2018**, *12* (1), 494−503.

(54) Kang, Y.-T.; Purcell, E.; Hadlock, T.; Lo, T.-W.; Mutukuri, A.; Jolly, S.; Nagrath, S. Multiplex Isolation and Profiling of Extracellular Vesicles Using a Microfluidic DICE Device. *Analyst* **2019**, *144* (19), 5785−5793.

(55) Cawley, J. L.; Blauch, M. E.; Collins, S. M.; Nice, J. B.; Xie, Q.; Jordan, L. R.; Brown, A. C.; Wittenberg, N. J. Nanoarrays of Individual Liposomes and Bacterial Outer Membrane Vesicles by Liftoff Nanocontact Printing. *Small* **2021**, *17* (50), 2103338.

(56) Kunding, A. H.; Mortensen, M. W.; Christensen, S. M.; Stamou, D. A Fluorescence-Based Technique to Construct Size Distributions from Single-Object Measurements: Application to the Extrusion of Lipid Vesicles. *Biophys. J.* **2008**, *95* (3), 1176−1188.

(57) Kato, S.; Kowashi, Y.; Demuth, D. R. Outer Membrane-like Vesicles Secreted by Actinobacillus Actinomycetemcomitans Are Enriched in Leukotoxin. *Microbial Pathogenesis* **2002**, *32* (1), 1−13.

(58) Dhurve, G.; Madikonda, A. K.; Jagannadham, M. V.; Siddavattam, D. Outer Membrane Vesicles of *Acinetobacter Baumannii* DS002 Are Selectively Enriched with TonB-Dependent Transporters and Play a Key Role in Iron Acquisition. *Microbiol Spectr* **2022**, *10* (2), No. e00293-22.

(59) Cooke, A. C.; Nello, A. V.; Ernst, R. K.; Schertzer, J. W. Analysis of Pseudomonas Aeruginosa Biofilm Membrane Vesicles Supports Multiple Mechanisms of Biogenesis. *PLoS One* **2019**, *14* (2), No. e0212275.

(60) Park, K.-S.; Choi, K.-H.; Kim, Y.-S.; Hong, B. S.; Kim, O. Y.; Kim, J. H.; Yoon, C. M.; Koh, G.-Y.; Kim, Y.-K.; Gho, Y. S. Outer Membrane Vesicles Derived from Escherichia Coli Induce Systemic Inflammatory Response Syndrome. *PLoS One* **2010**, *5* (6), No. e11334.